BOLLETTINO DI GEOFISICA TEORICA ED APPLICATA VOL. 45, N. 3, PP. 131-152; SEPTEMBER 2004

On the South Iceland earthquakes in June 2000: strong-motion effects and damage

R. SIGBJÖRNSSON and S. ÓLAFSSON

University of Iceland, Earthquake Engineering Research Centre , Selfoss, Iceland

(Received December 12, 2002; accepted June 6, 2003)

Abstract - The South Iceland earthquake sequence in June 2000 is discussed using available recordings from the Icelandic Strong-motion Network. The two largest events in the sequence occurred on 17 and 21 June, with surface-wave magnitudes of 6.6 and 6.5, respectively. Both were shallow, right-lateral, strike slip earthquakes on north-south striking faults. The attenuation of strong ground motion is analysed in terms of Arias intensity, rms and peak ground acceleration. Special emphasis is placed on near-source effects, as the shortest distances to the causative fault for recording stations are no more than a few km. The recorded near-source time series are characterised by very high acceleration but short duration. Furthermore, earthquake response spectra are discussed, both elastic and inelastic, emphasising strength and ductility demand. These spectra are viewed in the perspective of current seismic code as well as with respect to the observed earthquake-induced damage. The earthquake sequence in 2000 is also compared with noteworthy historic earthquakes in South Iceland, namely those in 1896 and 1912. The comparison is based on the total seismic moment and the size of the damage areas. The similarity between the 1896 and 2000 events is remarkable. In view of this and the high acceleration encountered, the damage in the epicentral areas is less than might have been expected. This is partly due to preparedness undertaken by individuals, municipalities and companies.

1. Introduction

The destructive South Iceland earthquakes in June 2000 are the most noteworthy seismic events in Iceland recorded by strong-motion instrumentation. The information obtained

Corresponding author: R. Sigbjörnsson, Earthquake Engineering Research Centre, Austurvegur 2a, IS-800 Selfoss, Iceland. Phone: +354 5254141; fax: +354 5254140; e-mail: ragnar.sigbjornsson@hi.is

contributes considerably to the understanding of the attenuation of seismic waves and to near-source effects of shallow, strike slip earthquakes. These data are now easily accessible through the ISESD project (Internet-Site for European Strong-Motion Data), supported by the European Commission, Research-Directorate General, Environment and Climate Programme (Ambraseys et al., 2002, 2003).

Iceland is widely known as a land of natural hazards, characterised by its volcanic activity, jokulhlaup (glacier bursts) and earthquakes. It is the most earthquake prone country in northern Europe. Annals and written documents, covering the last millennium, indicate that destructive earthquakes strike roughly twice every century. The physical effects of these earthquakes appear as surface fractures, landslides and rock-falls, changes in ground water levels, and disturbances of hot wells and springs. Furthermore, dwellings are severely damaged and are even shaken down and destroyed, building contents and inventory are ruined and domestic animals are killed. The social effects surface in psychological strain and injuries and, in a few cases, casualties. The economic effects are often long-term in nature and are hard to assess accurately. A remarkable comprehensive overview of the earthquake history of Iceland is found in the pioneering works of Thoroddsen (1899, 1925).

Iceland is a superstructural part of the Mid-Atlantic Ridge, a diverging plate boundary in the North Atlantic Ocean marking the border between the North American and the Eurasian Plates (see Fig. 1). Across Iceland from southwest to the north, the rift zone is displaced towards the east through two major fracture zones or transform faults. These are the South Iceland Seismic Zone (SISZ) and the Tjörnes Fracture Zone (TFZ), indicated on Fig. 1a. The size of earthquakes within these zones may reach magnitude seven or even more. Significant earthquakes outside these areas are often attributed to volcanic activity or geothermal processes. Intraplate tectonic earthquakes are also known. Volcanic earthquakes will rarely reach magnitude six. The geothermal-related earthquakes are small tremors that can be disturbing to exposed people but do not have significant effects on engineered structures. They rarely exceed magnitude three. Intraplate earthquakes have reached magnitude $5\frac{1}{2}$ (Einarsson, 1991).

Ambraseys and Sigbjörnsson (2000) have compiled available public domain data on earthquakes in Iceland and have given a comprehensive uniform account of the seismicity of the region. The earliest instrumental data on earthquakes in Iceland are from the great destructive South Iceland earthquakes in 1896, recorded by primitive seismographic stations in Russia and Italy. Along with the destructive 1912 earthquake, these earthquakes are the most noteworthy, instrumentally recorded events in the SISZ. The surface-wave magnitude of these events reached 6.6 and 7.0, respectively. In the last century, three destructive earthquakes struck coastal villages in North Iceland (TFZ) in 1934, 1963 and 1976. In addition, it is worth mentioning an earthquake occurring in 1910, which is the largest recorded earthquake in the Iceland area, reaching a surface-wave magnitude of 7.2.

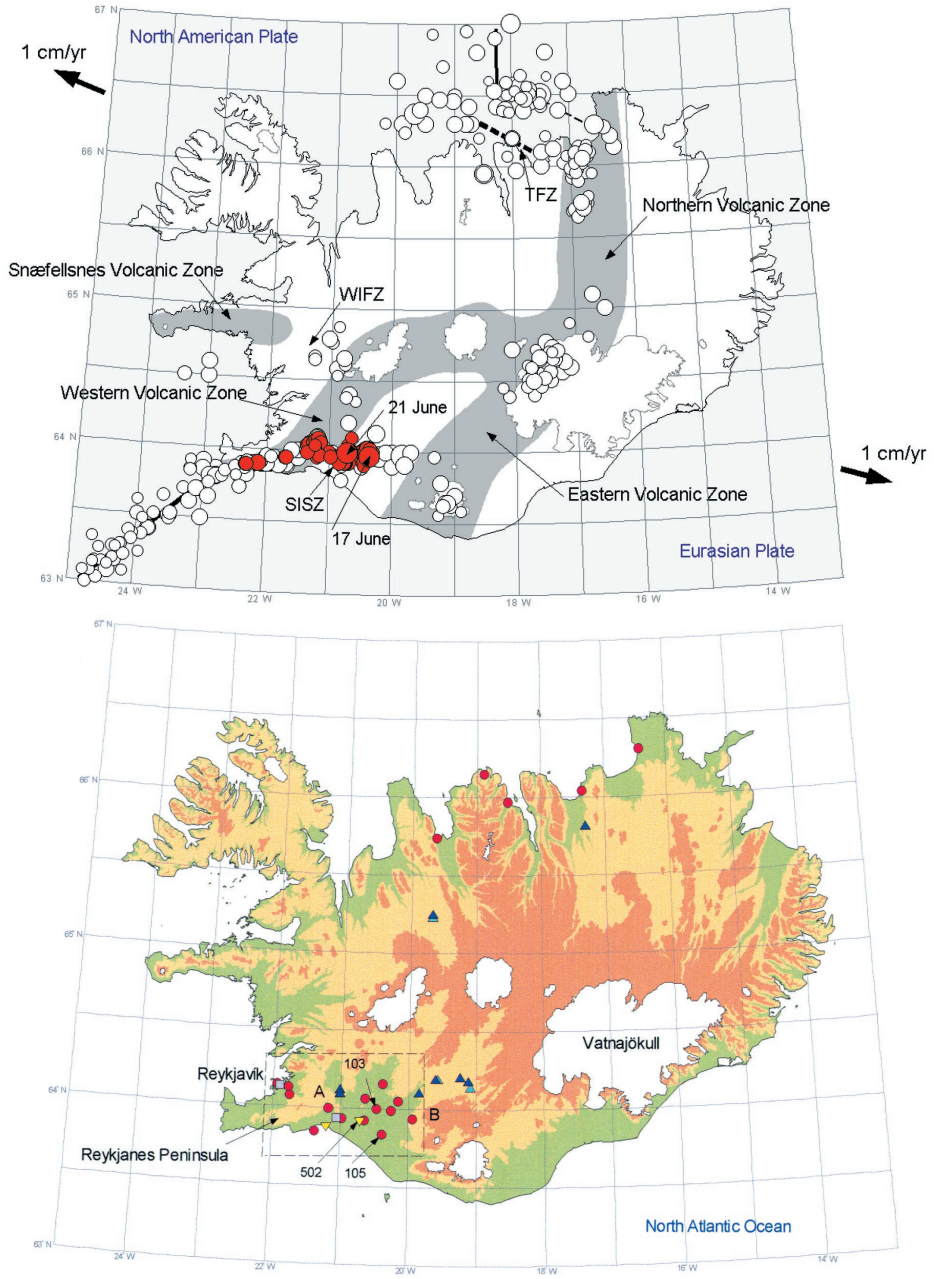

Fig. 1 - Overview. (a) Main tectonic structures and earthquake epicentres. The grey areas indicate volcanic zones; solid lines indicate rift zones offshore representing parts of the Mid-Atlantic Ridge; the rift zones on land are located at the Eastern, the Western and the North Volcanic zones; dashed lines indicates fracture zones offshore and seismic lineation; SISZ is the South Iceland Seismic Zone; TFZ is the Tjörnes fracture Zone; WIFZ is the West Iceland fracture Zone; white circles denote earthquake epicentres (Ambraseys and Sigbjörnsson, 2000); red circles show epicentres of events recorded by the Icelandic Strong-motion Network during the South Iceland earthquake sequence in June 2000; the average motion of the Eurasian Plate and North American Plate is indicated by the bold arrows. (b) The Icelandic Strong-motion Network. The following notation is used: ● ground response station; ▲ bridge; ■ building; ▲ power plant; ▲ earth fill dam. The rectangle marked by dashed lines indicates the study area shown on Fig. 2. Height above sea level is indicated using the following colour code: green 0-200 m; yellow 200-600 m; brown > 600 m. The white areas are glaciers. Note that the distance between the meridians at 63° parallel is ~ 50.5 km.

2. Strong-motion data

The Icelandic Strong Motion Network was initiated in 1984. It is based on a small-scale network proposed and installed by Professor Sólnes in the early seventies (Sigbjörnsson, 1990). The objectives of the network are to collect strong-motion data required for rational structural design and risk management. At present, the network consists of 34 permanent stations or subsystems (arrays) measuring ground motion and structural response. The stations comprise of 184 channels, which can be divided as follows: a) 22 standalone, triaxial ground response stations in farmhouses and public buildings (66 channels); b) 3 monitoring systems in earth-fill dams (30 channels); c) 5 monitoring systems in hydro-power stations (57 channels); d) 2 monitoring systems in office buildings (14 channels); e) 2 monitoring systems in seismically base isolated bridges (17 channels). The network runs with a high degree of automation, using digital instruments. The locations of the stations were selected on the basis of the geophysical information, the geographic distribution of the population and the locations of industrial and power plants as well as the main lifeline systems. In most cases the ground response stations are located inside buildings. There are two main reasons for this. Firstly, Iceland's severe climatic conditions make it difficult and expensive to operate sensitive equipment outdoors. Secondly, in order to comply with the above-mentioned objectives, it was judged important in interpreting and modelling earthquake action on structures and earthquake-induced structural response, that the obtained data represent the direct seismic effects on the structural foundations. In most cases, the building foundations are relatively stiff and have dimensions much smaller than the dominating earthquake wavelengths for the frequency range of main interest. It is therefore assumed that the recorded data represents free-field motion fairly well in most cases (Ambraseys et al., 2002).

The first major event recorded by the Icelandic Strong-motion Network was a magnitude 6 earthquake on 25 May 1987, with an epicentre in the Vatnafjöll Mountains south of Mt. Hekla (Ólafsson et al., 1998). Up to now nearly 300 events have been recorded. By far the most important seismic events recorded to date are the South Iceland earthquakes in June 2000.

The earthquake sequence started on 17 June 2000, 15:41, without any warning, with a moment magnitude 6.5 (M_W) earthquake (Ambraseys et al., 2002) in the eastern part of the SISZ. It was followed by great seismic activity stretching over an area more than 100 km long towards west, through the Hengill Area and along the Reykjanes Peninsula. This aftershock activity culminated in a magnitude 6.4 (M_W) event on 21 June, 00:51, (Ambraseys et al., 2002), with an epicentre approximately 17 km west of the epicentre of the first shock. The earthquakes occurred on N-S striking faults, transverse to the seismic zone. The sense of faulting was right-lateral strike slip in accordance with the model that the left-lateral E-W transform motion across the seismic zone is kinematically made possible through right-lateral motion along parallel N-S faults and by rotation of the blocks between them (Einarsson, 1991). The two largest earthquakes were accompanied by 20 km long surface faulting characterised by interchanging echelon gashes and push-up structures. The largest earthquakes, which were felt in most of Iceland, caused great damage to structures, building contents and house articles, but there were no fatalities. The structural damage was most severe in older buildings, buildings raised on poor

foundations, buildings made of masonry or building blocks of lava aggregate, buildings with masonry partitions and buildings with 'floating' concrete slabs on earth fill. Also, many non-reinforced or scarcely reinforced concrete buildings were greatly damaged, especially outbuildings in rural areas. Significant damage occurred to communication structures in the epicentral area.

In total, the Icelandic Strong-motion Network recorded 83 events in June 2000 and in the following months, resulting in 774 ground response time series. The two largest events, on 17 June and 21 June, were recorded at every station within a radius of 150 km. In these two events 147 ground response time series were recorded. The highest peak ground acceleration (PGA) measured in the first earthquake was about 64% g at Station 103, in the basement of a building in Holt. In the latter earthquake, the highest PGA measured was approximately 84% g on the west pillar of the Thjórsá River Bridge (Station 502, see Fig. 1). The epicentral distance was in the range of 5 to 270 km, and the shortest distance to the surface trace of the earthquake fault was no more than a couple of km.

Figs. 2 and 3 display an overview of the time series recorded in the two largest events on 17 and 21 June 2000, respectively. The locations of the recording stations, using geographical coordinates, are indicated by squares. The accelerations are shown on Figs. 2a-2c and 3a-3c while the corresponding velocities are plotted on Figs. 2d-2f and 3d-3f. The horizontal components are denoted by x and y while the vertical direction is indicated by z. It should be noted that the x- and y-direction do not strictly follow the geographical directions. The causative faults are indicated on the figures. It is seen that some of the stations are close to the faults. It is especially worth noting Stations 107 (Thjórsártún) and Station 109 (Sólheimar) where the recordings on the 21 June show a significant near-field pulse (see Fig. 3).

Some basic knowledge of the geology of the South Iceland Lowland is needed for the interpretation of the strong-motion data. The surface geology is mostly formed during and after the last ice age as a pile of basaltic lavas, as well as tuff layers, often with intermediate layers of sediments or alluvium. The youngest lavas are from the Holocene (not more than couple of hundred years old), while the oldest formations are up to 3.3 million years old. In the glacial period Iceland was covered with a plateau glacier. During warmer interglacial periods the ice melted and the glaciers retreated, which resulted in sea level changes up to couple of hundred meters. The South Iceland Lowland was then partly a seabed, accumulating marine sediments. During warm periods, and towards the end of the Pleistocene, when the glacier was retreating and the land rising, glacial streams formed thick sediment layers, composed chiefly of sand and fine-grain gravel. In the postglacial period, some of these sediments were covered by lava, which adds to the complexity of the geological structure of the surface. The lava layers may be as thick as 10 m while the sediment layers can be up to 20 m thick or even more (Einarsson, 1994). The shear wave velocity in basaltic rock is typically in the range 2 to 2.8 km/s, depending on how dense the rock are, while the shear wave velocity in tuff and sedimentary rock is, respectively, 850 m/s and 1000 m/s on the average.

The complexity of the surface geology, characterised by the lava piles, tuff and sedimentary formations, is augmented further by fractures, fissures and faults of tectonic origin. These intricacies tend to increase earthquake-induced effects as already noticed in the 1896 destructive

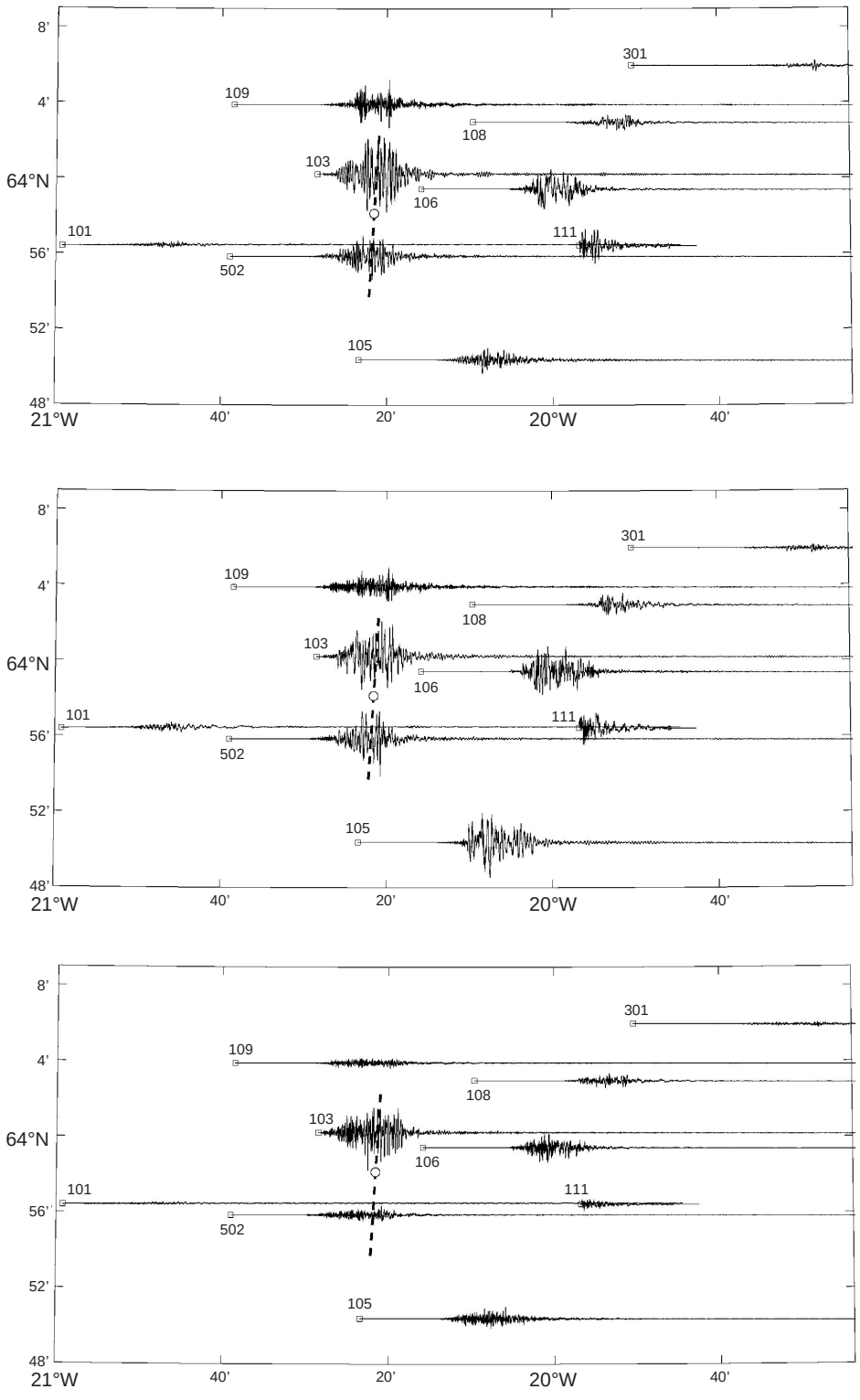

Fig. 2 - Ground motion on 17 June 2000, 15:41: a) x-component of acceleration, b) y-component of acceleration, c) z-component of acceleration, d) x-component of velocity, e) y-component of velocity, f) z-component of velocity. The causative fault is indicated by dashed line; and the corresponding epicentre is shown as open circle.

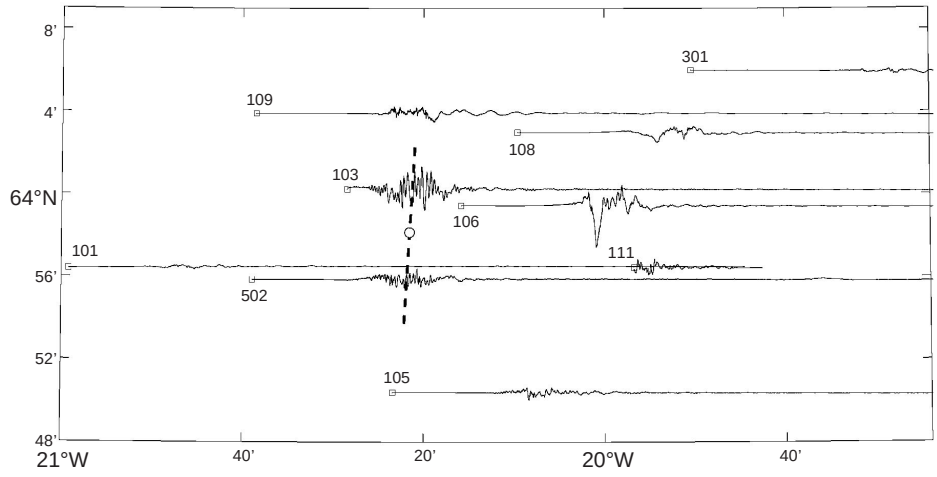

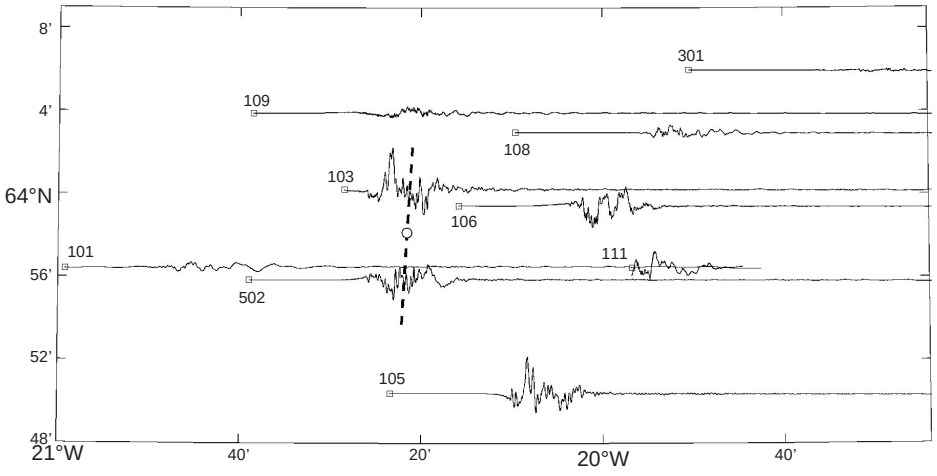

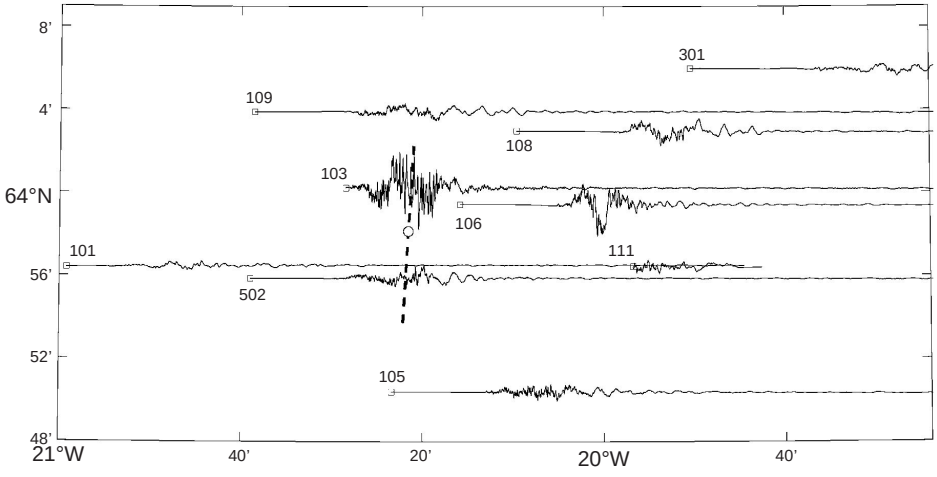

Fig. 2 - continued.

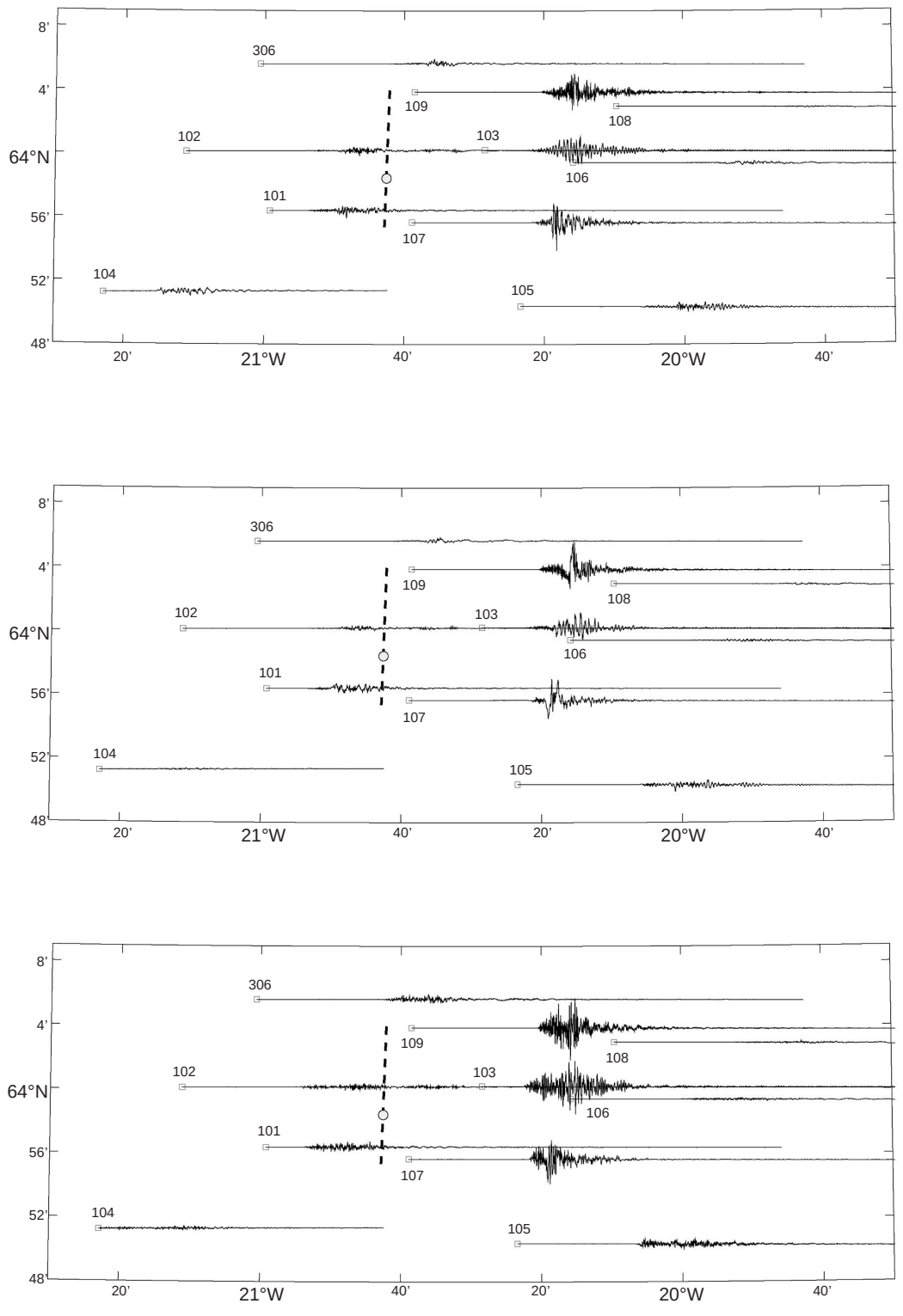

Fig. 3 - Ground motion on 21 June 2000, 00:52: a) x-component of acceleration, b) y-component of acceleration, c) z-component of acceleration, d) x-component of velocity, e) y-component of velocity, f) z-component of velocity. The causative fault is indicated by dashed line; and the corresponding epicentre is shown as open circle.

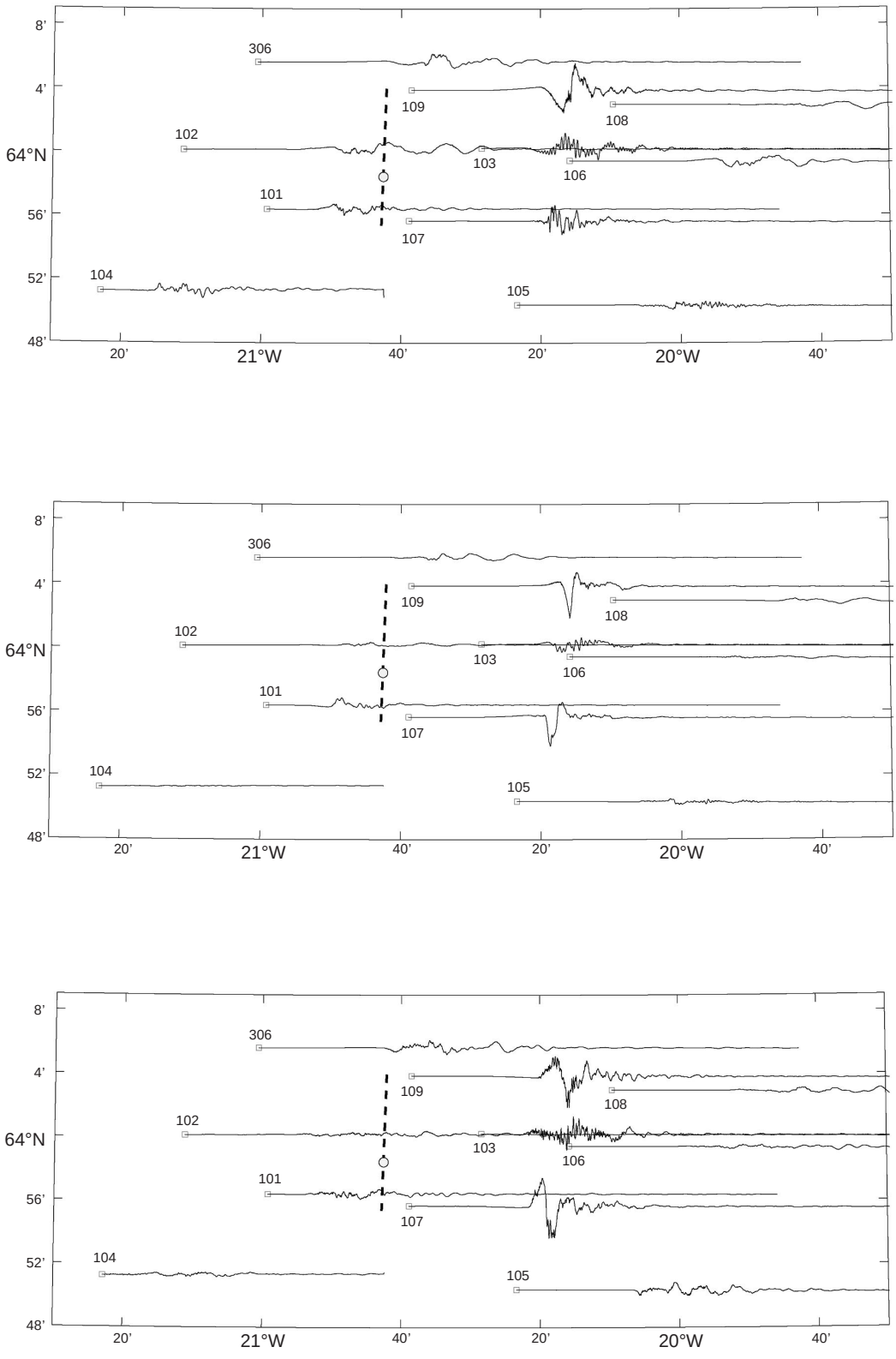

Fig. 3 - continued.

earthquakes (Thoroddsen, 1899). The ground response stations are classified according to Boore et al. (1993) classification scheme. The majority of the stations fall into the rock class ($v_{s,30}$ > 750 m/s) leaving only two station (109 and 111) in the stiff soil class (360 m/s < $v_{s,30}$ < 750 m/s). This classification should, however, be treated with some caution due to the inherent complex geological structure outlined above. Further studies into the classification of the stations are therefore in progress.

3. Analysis

The Brune model (Brune, 1970) has been applied successfully to analyse Icelandic earthquakes and strong-motion data (Ólafsson et al., 1998, 2001; Ólafsson, 1999; Ólafsson and Sigbjörnsson, 1999, 2002). This model will also be used in the following analysis of attenuation and near source effects. First some preliminaries of the modelling will be reviewed and the applied formulas stated.

3.1. Modelling

The Brune model for seismic shear waves was derived by considering the effective stress needed to accelerate the sides of a circular causative fault on which a stress pulse is applied instantaneously (Brune, 1970, 1971). It is commonly used to obtain fault dimensions from spectra of shear waves for small to moderate sized earthquakes (Udias, 1999). The model describes near- and far-field displacement-time functions as well as spectra and includes the effect of fractional stress drop. The near-field amplitude displacement spectrum is given as (Brune, 1970):

$$|D(\omega)| = \frac{\sigma\beta}{\mu}\frac{1}{\omega\sqrt{\omega^2 + \tau^{-2}}}\ , \tag{1}$$

while the far-field rms displacement spectrum can be expressed as follows (Brune, 1970):

$$\langle D(\omega)\rangle = \langle R_{\theta\phi}\rangle\ \frac{\sigma\beta}{\mu}\ \frac{r}{R}\frac{1}{\omega^2 + \omega_c^2}\ . \tag{2}$$

Here, $\langle R_{\theta\phi}\rangle$ is the rms average of the radiation pattern, denotes frequency in rad/s, β is the shear wave velocity, μ is the shear modulus, r is the radius of the circular fault, R is the distance from source to site, ω_c and τ are model parameters, respectively, the corner frequency and rise-time, given as (Brune, 1970, 1971):

$$\omega_c = \sqrt{\frac{7\pi}{4}}\frac{\beta}{r} \tag{3}$$

and

$$\tau = O\,(r/\beta)\,, \tag{4}$$

where the Landau symbol O indicates the properties of the functional relationship. Finally, σ denotes the effective stress. If the effective stress does not drop to zero but only to a fraction of complete stress drop, the rise-time and high-frequency spectra are modified especially in the long-period range (see Brune, 1970).

In the above mentioned studies of Icelandic earthquakes it is assumed that the effective stress equals the stress drop, i.e. $\sigma = \Delta\sigma$, where $\Delta\sigma$ denotes the stress drop. For a double couple source it can be shown that the stress drop is related to the seismic moment, M_o, through (see, for instance, Udias, 1999):

$$\Delta\sigma = \frac{7}{16}\,\frac{M_o}{r^3}\,, \tag{5}$$

Furthermore, it is assumed that the acceleration spectrum can be derived from the displacement spectrum by introducing an exponential term to account for spectral attenuation at high frequencies (Anderson and Hough, 1984; Ólafsson, 1999):

$$|A\,(\omega)| = \omega^2\,|D\,(\omega)|\,\exp\,(-\tfrac{1}{2}\,\kappa\omega)\,, \tag{6}$$

where κ is the so-called spectral decay parameter. The spectral decay parameter is related to the quality factor Q through the following equation:

$$\kappa = \frac{R}{\beta Q}\,. \tag{7}$$

The quality factor, Q, is in this context assumed to represent the average scattering and anelastic attenuation over the whole path. Studies of Icelandic strong-motion data indicate that the spectral decay, κ, can be taken as constant (Ólafsson, 1999), at least for moderate epicentral distances, where the seismic wave field is dominated by shear waves and the Brune model is assumed to hold as an engineering approximation. The slow increase of κ with distance found by Anderson and Hough (1984) is not observed in the available Icelandic data (Ólafsson, 1999). This implies that the quality factor Q varies approximately linearly with increasing distance from the source. This seems consistent with the fact that sites at great distance from the source are receiving shear waves that have penetrated through lower crustal layers with less attenuation than the upper layers.

The acceleration spectrum in the far-field can hence be expressed as follows, accounting for the free-surface effects and partitioning of the wave energy into two horizontal components (Ólafsson, 1999):

$$|A(\omega)| = \frac{2C_P R_{\theta\phi} M_o}{4\pi\beta^3\rho R} \frac{\omega^2}{(1 + (\omega / \omega_c)^2)} \exp(-\tfrac{1}{2}\kappa\omega) . \tag{8a}$$

Here, C_P is the partitioning factor, $R_{\theta\phi}$ denotes the radiation pattern and ρ is the material density of the crust. The following expression is suggested for the geometrical spreading function (Ólafsson, 1999):

$$R = \begin{cases} D_2^{1-n} D^n & D_1 < D \le D_2 \\ D & D_2 < D \le D_3 \end{cases}, \tag{8b}$$

where $1 < n \le 2$ and R is a distance defined as:

$$D = \sqrt{d^2 + h^2} . \tag{8c}$$

Here, d is the epicentral distance and h is a depth parameter. The parameters D_1, D_2 and D_3 are used to set the limits for the different zones of the spreading function. The first zone can be thought of as a crude approximation for the intermediate field. Hence, the quantity D_1 can be approximated by h; D_2 quantifies the size of the zone representing the intermediate field, which is related to the magnitude of the earthquake (as represented by the seismic moment) and the thickness of the seismogenic zone; while D_3 can be thought of as the distance where cylindrical waves begin to dominate the wave field.

The time domain properties of acceleration, a, can readily be derived from the Fourier spectrum, A, by applying the Parseval theorem. This gives:

$$I = \int_0^T a^2(t)\, dt = \frac{1}{2\pi} \int_{-\infty}^{\infty} |A(\omega)|^2 \, d\omega . \tag{9}$$

The last integral can be evaluated after substituting Eq. (8). The result is:

$$I = \frac{\left(2\sqrt{7}\right)^{4/3}}{4\pi} \left(\frac{C_P R_{\theta\phi} \Delta\sigma^{2/3}}{\beta\rho R} \right)^2 \frac{\Psi}{\kappa} M_0^{2/3} , \tag{10}$$

where Ψ denotes a dispersion function given by the following integral for which a closed form solution is readily obtained:

$$\Psi = \lambda \int_0^{\infty} \frac{\varpi^4}{(1 + (\varpi^2)^2} \, \mathrm{e}^{-\lambda\varpi} \, d\varpi , \tag{11a}$$

$$\Psi = 1 - \frac{1}{2}\lambda\, ci(\lambda)\,(\lambda\, cos(\lambda) + 3\, sin(\lambda)) - \frac{1}{2}\lambda\, si(\lambda)\,(\lambda\, sin(\lambda) - 3\, cos(\lambda)) . \tag{11b}$$

Here, $ci(\cdot)$ and $si(\cdot)$ represent the cosine and sine integrals, respectively, $\varpi = \omega / \omega_c$ and:

$$\lambda = \kappa\, \omega_c\,, \tag{12}$$

where ω_c is the corner frequency. The sine and cosine integrals applied in Eq. (11) are given, respectively, as follows:

$$\begin{aligned} si(\lambda) &= -\frac{\pi}{2} + \int_0^{\lambda} \frac{sin(t)}{t} dt\,, \\ ci(\lambda) &= \gamma + ln(\lambda) + \int_0^{\lambda} \frac{cos(t)}{t}\ dt\,, \end{aligned} \tag{13}$$

where γ is the Euler constant ($\gamma \approx 0.5772$).

3.2. Arias intensity

To get a unified measure of strong-motion intensity, reflecting both the size and duration of the acceleration, it is feasible to use Arias intensity. The Arias intensity tensor, I_{ij}, is defined formally as (Arias, 1970):

$$I_{ij} = \frac{\pi}{2g} \int_0^T a_i\,(t)\; a_j\,(t)\; dt\,, \tag{14}$$

where $a_i(t)$ and $a_j(t)$ refer to the *ith* and *jth* component of the ground acceleration, respectively, ($\{i, j\} \in \{x, y, z\}$), T is the duration of the recordings, and g is the acceleration due to gravity. This leads to the following far-field attenuation formula for the Arias intensity, I_A, of the horizontal components:

$$log_{10}\,(I_A) = log_{10} \left(\frac{\left(2\sqrt{7}\right)^{4/3}}{8\,g} \left(\frac{C_P\, R_{\theta\phi}\, \Delta\sigma^{2/3}}{\beta\rho\sqrt{\kappa}} \right)^2 \Psi \right) + \frac{2}{}\ log_{10}\,(M_o) - 2\ log_{10}\,(R)\,. \tag{15}$$

Here $I_A \in \{I_{xx}, I_{yy}\}$, where x and y refer to the horizontal axis, respectively. The results are indicated in Fig. 4. Here, we see the Arias intensity of the horizontal components related to the corresponding PGA. The relation between Arias intensity and PGA has been studied. On a log-log scale, the relation is highly linear with a coefficient of determination equal to 0.91.

3.3. Attenuation of rms and PGA in the far-field

The rms ground acceleration can be defined as follows:

$$a_{rms} = \sqrt{\frac{1}{T_d} \int_0^{T_d} a^2\,(t)\; dt}\,, \tag{16}$$

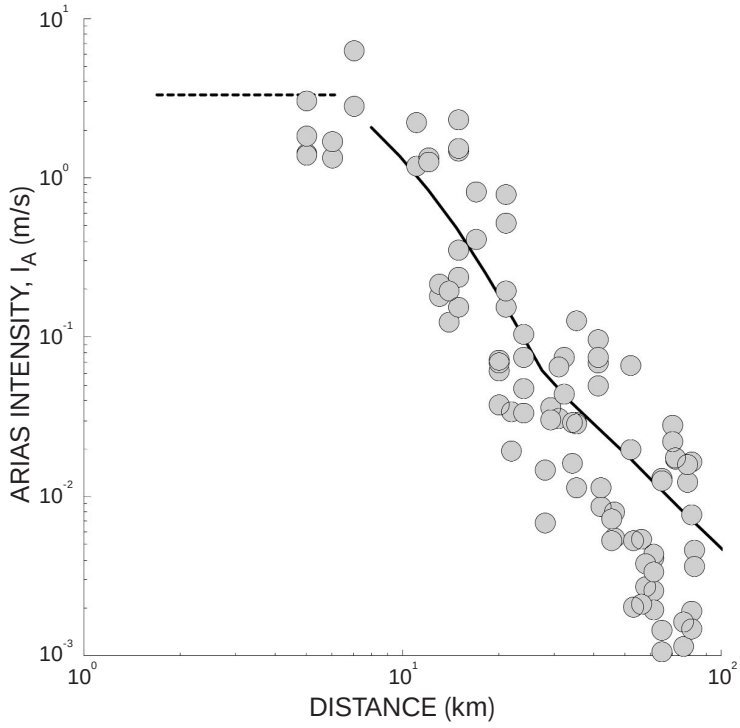

Fig. 4 - Attenuation of Arias intensity for horizontal motion. The solid curve represents the far- and intermediate-field model, the horizontal dashed curve gives the near-field model, and circles represent data from the South Iceland earthquakes on 17 and 21 June 2000.

where T_d is the duration of shaking. A closed form attenuation formula can be derived using the Parseval theorem and Eqs. (16) and (10) above. It is:

$$log_{10}\,(a_{rms}) = log_{10}\left(\frac{\left(2\sqrt{7}\right)^{2/3}}{2\sqrt{\pi}}\frac{C_P\,R_{\theta\phi}\,\Delta\sigma^{2/3}}{\beta\rho\sqrt{\kappa}}\right) + \frac{1}{2}\,log_{10}\left(\frac{\Psi}{T_d}\right) + \frac{1}{3}\,log_{10}\,(M_o) - log_{10}\,(R)\,. \quad (17)$$

The PGA can be related to the rms ground acceleration by applying the theory of locally stationary Gaussian processes (Vanmarcke and Lai, 1980). The result is:

$$a_{peak} = p a_{rms}\,, \quad (18)$$

where p is the so-called peak function, which depends on the strong motion duration, T_d, and the predominant period of the strong motion phase of the acceleration (Vanmarcke and Lai, 1980; Hanks and McGuire, 1981; Boore 1983). This relation has been shown to hold for the available Icelandic strong-motion data (see, for instance, Ólafsson, 1999). Hence, the same functional form as used for the rms value can describe attenuation of the PGA. The results are indicated in Fig. 5.

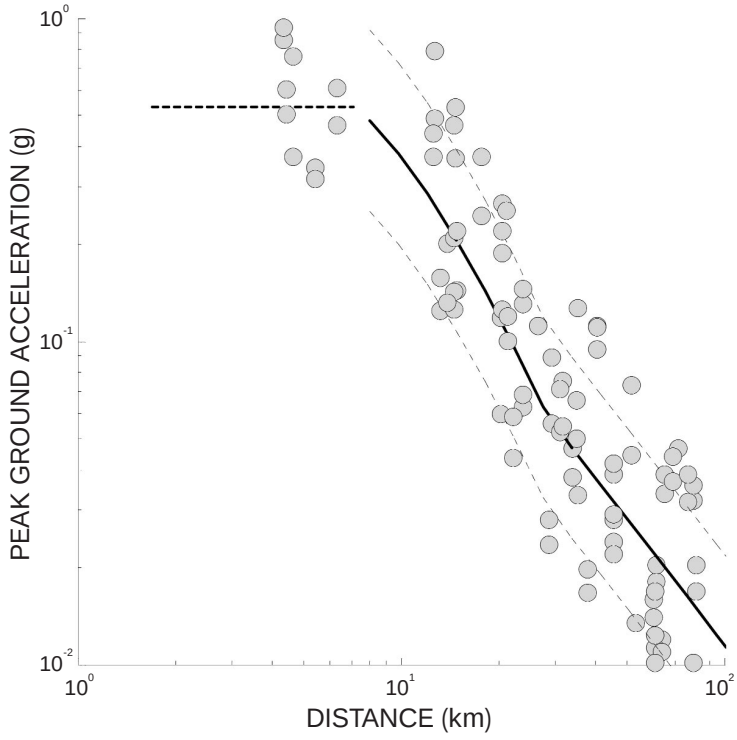

Fig. 5 - Attenuation of horizontal PGA. The solid curve represents the far- and intermediate-field model, the horizontal dashed curve gives the near-field model, and the circles represent data from the South Iceland earthquakes on 17 and 21 June 2000. Dotted curves indicate the deviation of the data from the model by ± one standard deviation.

3.4. Rms and PGA in the near- field

The model described in the previous section is not valid in the near-field and can, therefore, not be expected to describe the PGA accurately close to the fault. To be able to obtain an approximation valid for shear waves in the near-fault area, it is suggested that the Brune near-field model, Eq. (1), is used. Hence, the near-field acceleration spectrum can be approximated as follows, accounting for the free surface and partitioning of the energy into two horizontal components:

$$|A(\omega)| = \frac{7}{8}\frac{C_p M_o}{\rho\beta r^3}\frac{\omega}{\sqrt{\omega^2 + \tau^{-2}}}\exp\left(-\tfrac{1}{2}\kappa_o\,\omega\right). \tag{19}$$

Here, κ_o is the spectral decay of the near-field spectra. Otherwise the same notation is used as above. An approximation for the rms and PGA is now obtained by applying the Parseval theorem and, then, carrying out the integration. The result is:

$$log_{10}(a_{rms}) = log_{10}\left(\frac{1}{\sqrt{\pi}}\frac{7}{8}\frac{C_p}{\rho\beta r^3\sqrt{\kappa_o}}\right) + \frac{1}{2}\,log_{10}\left(\frac{\Psi_o}{T_o}\right) + log_{10}(M_o). \tag{20}$$

Here, the duration is denoted by T_o and Ψ_o is a dispersion function given as:

$$\Psi_o = \lambda \int_0^\infty \frac{\varpi^2}{1+\varpi^2} e^{-\lambda\varpi} d\varpi, \tag{21a}$$

$$\Psi_o = 1 - \lambda\,(ci(\lambda)\,sin(\lambda) - si(\lambda)\,cos(\lambda)), \tag{21b}$$

where $\lambda = \kappa_o / \tau$. It is seen that the PGA predicted by this equation is independent of the epicentral distance and hence should give an estimate on the upper-bound of PGA. Another result, which emerges when Eq. (5) is substituted into Eq. (20), is that the rms acceleration is directly proportional to the stress drop. That is:

$$a_{rms} = \frac{2}{\sqrt{\pi}} \frac{C_p\,\Delta\sigma}{\rho\beta\sqrt{\kappa_o}} \sqrt{\frac{\Psi_o}{T_o}}. \tag{22}$$

This indicates that assuming constant stress drop the ground acceleration in terms of the rms value can decrease with increasing earthquake magnitude.

4. Discussion

The most intensive damage to buildings and structures was confined to elongated areas around the causative faults of the two largest events (see Table 1). This is in agreement with strong-motion data represented by Arias intensity and PGA (see Figs. 1 and 2). The strong motion shows great variability in the near-fault area with PGA-values ranging from 0.3 g up to 0.8 g. For distances greater than 15 to 20 km, the PGA, on the other hand, has attenuated to below 0.2 g [see Ambraseys et al. (2002), for further details].

The attenuation of the Arias intensity for the horizontal components of motion is displayed in Fig. 4. The data from the earthquakes on 17 and 21 of June are applied but have been scaled to fit the seismic moment of the 17 June earthquake. The far- and intermediate-field model is represented by the black curve while the near-field model is represented by the horizontal dashed curve. Following data are assumed: shear wave velocity, β = 3.5 km/s; density of rock, ρ = 2.8 g/cm^3; stress drop, $\Delta\sigma$ = 100 bar; average radiation pattern, $R_{\theta\phi}$ = 0.63; partitioning parameter, $C_P = 1/\sqrt{2}$; peak factor, p = 2.94; spectral decay in the far-field, κ = 0.04 s, characteristic dimension of the intermediate-field, R_2 = 30 km; depth parameter, h = 9 km; exponent describing attenuation in the intermediate-field, n = 2; spectral decay in the near-field, κ_o = 0.04 *s*; characteristic fault dimension (radius), r = 8.0 km; duration used in near-field model, $T_o = 1.5 \cdot r / \beta$. These source data give average slip equal to 1.5 m, which seems in fair accordance with more refined estimates. It is seen that the Arias intensity attenuates very rapidly, and more rapidly than the PGA. This supports the hypothesis that the damaging potential of these earthquakes attenuates more rapidly than indicated by the PGA alone. The theoretical model, given by the black curve in Fig. 4, fits the empirical data reasonably well.

Table 1 - Comparison of South Iceland earthquakes in August and September 1896, May 1912 and June 2000.

Event / Date	Origin time (GMT)	Epicentre		Damage area (km^2)	Magnitude (M_S)	Seismic moment (EN_m)
		°N	°W			
South Iceland Earthquakes 1896						
26 August	23:20	63.97	20.20	528	6.62	11.0
27 August	10:47	64.13	20.25	-	6.12	2.4
5 September	23:57	63.98	20.70	220	6.35	4.8
6 September	-	63.98	21.20	41	-	-
10 September	-	63.95	20.85	-	-	-
Total damage area 1896				789		
Total seismic moment 1896						18.2
South Iceland Earthquake 1912						
6 May	18:59	63.98	19.83	717	7.05	45.6
Total damage area 1912				717		
Total seismic moment 1912						45.6
South Iceland Earthquakes 2000						
17 June	15:41	63.97	20.36	438	6.60	10.2
17 June	15:43	63.95	20.46	-	(5.50)	0.7
17 June	15:45	63.90	22.13	-	-	-
17 June	15:46	63.96	20.37	-	-	-
17 June	17:09	64.04	21.35	-	-	-
17 June	17:40	63.98	20.72	-	-	-
21 June	00:52	63.98	20.71	358	6.50	7.6
21 June	00:55	63.97	20.66	-	-	-
Total damage area 2000				796		
Total seismic moment 2000						18.5

The necessity of accounting for the above-mentioned near-source effects, which are significant for distances shorter than 10 km, is obvious. It is also seen that the near-field model, represented by the horizontal dashed curve in Fig. 4, gives apparently fair upper bound for the Arias intensity.

The results obtained for the horizontal PGA are displayed in Fig. 5 including data from the two above-mentioned earthquakes as well as for the same model parameters used earlier. The model for the far- and intermediate-fields, represented by the solid black curves, is seen to fit the data reasonably well. Furthermore, the near-field model, given by the dashed curve, appears to give sensible values for the near-fault accelerations. It is worth pointing out that the formula for PGA fits the data considerably better than the formula for Arias intensity as well as the rms formulas. This seems in accordance with results reported in the literature (Ólafsson, 1999).

4.1. Elastic and inelastic earthquake response spectra and damage

Linear, elastic earthquake response spectra are given on ISESD (Ambraseys et al., 2002), where the pseudo-velocity, displacement and pseudo-acceleration are displayed as a function of undamped natural period for critical damping ratios equal to 2%, 5%, 10% and 20%, respectively. In the near-fault area the linear acceleration spectra indicate that the base shear

may be as high as 3 to 4 times the acceleration of gravity, while the vertical acceleration is of the same order of magnitude, e.g. Station 103 (Kaldárholt), approximately 5 km to the west of the causative fault on 17 June 2002, 15:41, and Station 105 (Hella), approximately 5 km towards south of the causative fault. This implies that the behaviour of real structures in the near-fault area cannot be predicted by linear models, especially as the seismic design requirements are rather weak in general and non-existent for older buildings. Hence, to assess the required strength demand, inelastic spectra are calculated. The results are displayed in Fig. 6 for the two above-mentioned recording stations. Only horizontal action is considered. The figures show the ductility demand for a prescribed strength, corresponding, respectively, to seismic coefficients equal to 0.4 g and 0.6 g. The dotted curves, indicating the linear displacement spectra for 5% critical damping ratio, are inserted for comparison. They are obtained by dividing the linear displacements by a yield displacement equal to f_u / ω^2, where f_u is the yield strength and ω is the undamped natural frequency in rad/s. It is seen that the frequency of characteristic peak in the linear spectrum is lower for Station 105, about 2.2 Hz, than for Station 103, about 3.3 Hz. This lower frequency encountered at Station 105 seems to be site-specific, at least to a certain extent. The non-linear spectra show, in both cases, a well-known shift in the characteristic spectral peaks. The shift is encountered for the weaker systems towards higher frequencies, relative to the characteristic peaks in the spectra for the stronger systems. These spectra indicate that buildings designed according to the minimum requirements of current seismic code (see below) are bound to suffer severe damage, which surfaces as cracks in the concrete and masonry partitions, yielding in reinforcements and excessive deformations in timber elements.

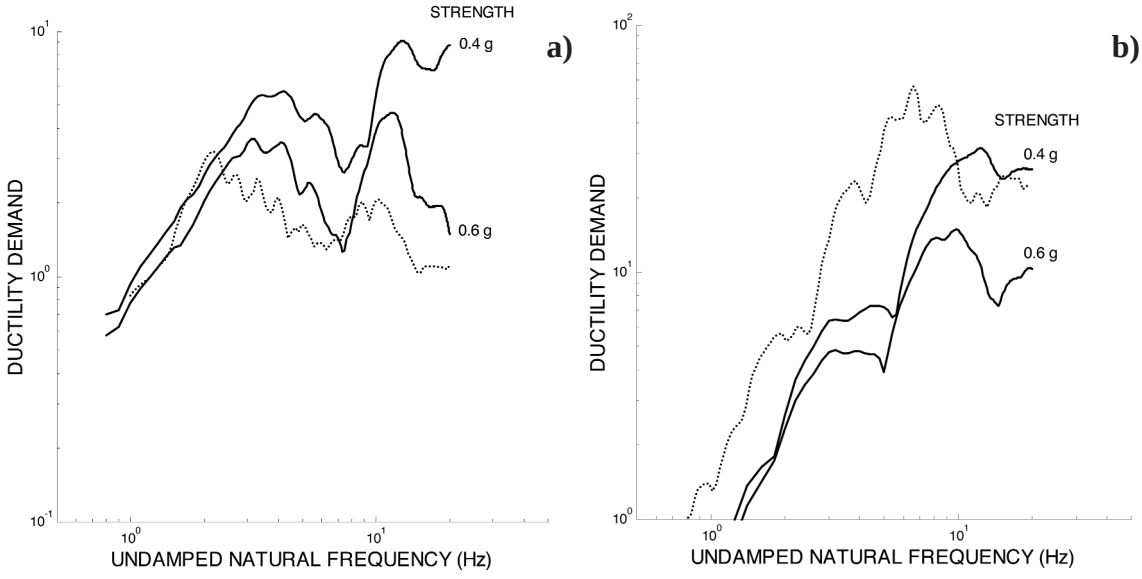

Fig. 6 - Earthquake response spectra for the South Iceland earthquake on 17 June 2000, 15:41. Solid curves indicate inelastic earthquake response spectra for constant strength and dashed curve gives the linear elastic earthquake response spectra scaled by the yield displacement for a system with strength of 0.6 g. (a) E-W component at Station 105 and (b) N-S component at Station 103.

The strength demand as a function of the ductility demand is displayed in Fig. 7 for the above-mentioned recording stations. Only structures with undamped natural frequency equal to 2, 5 and 10 Hz, respectively, are considered. On the average we see that the strength demand decreases with increasing ductility demand. The figure displays, however, some characteristic differences also seen in Fig. 6. The curve for a structure with a 10 Hz natural frequency at Station 103 is considerably higher than the corresponding curve for Station 105. This can be attributed to the spectral characteristics of the ground acceleration reflected in the higher dominating frequency at Station 103 than 105. It is also seen that the strength demands for 2 and 5 Hz structures tend to be higher than for 10 Hz structures if the ductility is higher than 2. This is not the case for Station 103 where the strength demand tends to decrease with decreasing natural frequency of the structure. In that case the curves show characteristic humps, which are related to the increased flexibility of the yielding system and its relation to the dominating frequency of the excitation. Such humps may appear when the system's flexibility increases gradually with increasing yielding, resulting in a lower effective frequency, that eventually moves out of the frequency band where the highest excitation energy is contained. This explains why such humps are not seen in the graphs for Station 105 for the ductility range considered. Fig. 7 shows that strength demand is very high for both records, for low ductility ratio. Furthermore, it is seen that for strength corresponding to a seismic coefficient equal to one g, the ductility demand may be in the range of 1.5 to 2 for structure with undamped natural periods above about 10 Hz.

When the damage in the epicentral area is assessed, it is necessary to take into consideration that many of the structures are built without any seismic provisions, and that the codified seismic design demand in this region is only about 20% g. This value refers to horizontal action, as vertical action is not taken into consideration. Hence, it may seem surprising that the damage to buildings was not more severe than it turned out to be in reality (see Figs. 3 and 4). The reasons for this may be many. The buildings in the area, which are made of concrete, masonry

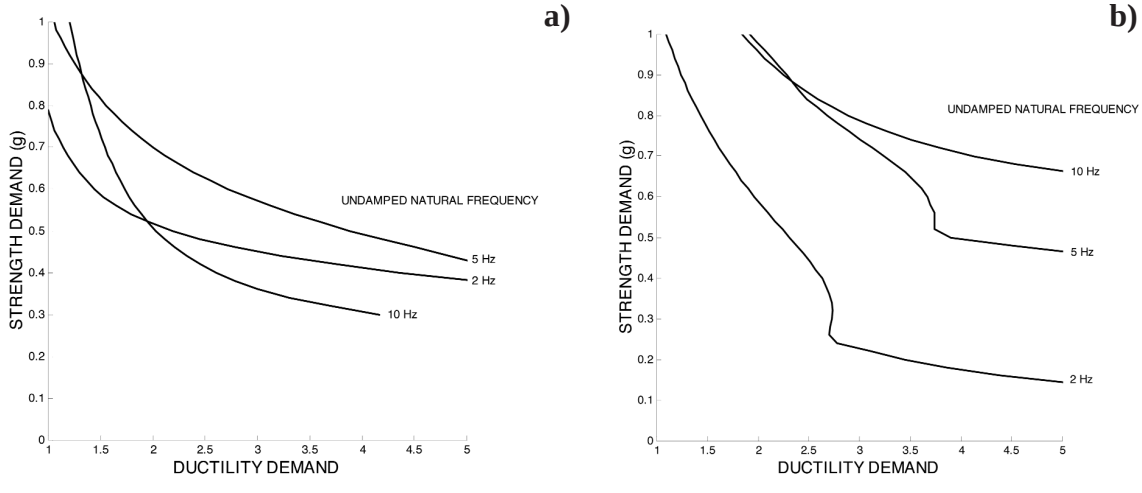

Fig. 7 - Strength demand as a function of ductility demand for inelastic systems with undamped natural frequencies equal to 2, 5 and 10 Hz during the South Iceland earthquake on 17 June 2000, 15:41. (a) E-W component at Station 105 and (b) N-S component at Station 103.

and timber, can be characterised as low-rise, with no buildings exceeding three storeys. The fundamental natural frequencies of these buildings are, in most cases, of the order of 10 Hz and almost in no cases are they below 5 Hz. It seems obvious that the high natural strength of these low-rise buildings is a key factor. This high strength is first of all attributed to other design considerations than the rather weak seismic design requirements. Furthermore, it seems clear (see Fig. 7, Station 105) that the spectral characteristics of the earthquake action are, at least in some cases, favourable to stiff, low-rise buildings compared with more flexible multi-storey buildings. In addition, it is obvious, when the damage of building is analysed, that the short duration of strong shaking contributed to the survival of the structures. There is no doubt that longer duration shaking would have inevitably led to collapse of several buildings. Repeated earthquake activity, indicated above (see also Table 1), had, on the other hand, negative effects on the buildings that appeared as progressive damage and crack growth.

4.2. Comparison to historic earthquakes

When the first earthquake struck there was a lot of confusion. The official assessment of magnitude was initially far too low and the event was rejected by some people as being a part of a South Iceland earthquake sequence (commonly defined as a damaging sequence including events of magnitude in the range 6 1/2 to 7). Therefore, it was useful to compare the sequence with some important historic earthquakes in the area by applying total seismic moments and size of damage zones. The calculations are based on available data and a relation between magnitude and seismic moment presented by Ambraseys and Sigbjörnsson (2000).

The results are summarised in Table 1. It should be noted that the applied magnitude of the largest events in 2000 are slightly higher than reported by some agencies. Furthermore, the seismic moments derived from the surface-wave magnitude are somewhat higher than the CMT values reported in ISESD (Ambraseys et al., 2002). Such direct assessment of the seismic moments is however not available for the historic earthquakes, and therefore to maintain consistency it was decided to base the calculations on the estimated surface-wave magnitudes and their derived seismic moments.

In general, it is difficult to define a damage area with precision. The damage area for the historic earthquakes is defined as the area where more than half of the buildings, mostly traditional Icelandic houses, collapsed. This definition has been adopted for the 2000 earthquakes even though it is not straightforward due to increased robustness of modern buildings in comparison with the vulnerable, traditional buildings, which dominated the settled area in earlier times. It should be further noted that the damage areas are in some cases overlapping, which makes an exact determination of their size not easy.

Examining Table 1, it is seen that the South Iceland earthquakes in 2000 are comparable to the 1896 earthquakes, with respect to both total seismic moment and the size of the damage areas. It should be noted that in the table, three earthquakes contributed to the total seismic moment in 1896. In this context, it is worth pointing out that the earthquake on 5 September 1896 in reality comprised of two separate events with clearly separated damage areas

(Thoroddsen, 1899; Ambraseys and Sigbjörnsson, 2000). On the other hand, there are only two events in 2000 that contributed significantly to the total moment. The earthquake in 1912 may seem to be of a different nature in the sense that it is only a single event, but its seismic moment is more than twice the total moment in the events of 1896 and 2000.

5. Conclusion

When the effects of the South Iceland earthquakes in 2000 are assessed, and the destruction following in their wake is analysed, it can be said that the inhabited areas in South Iceland came through fairly well and better than one would have expected, considering the high acceleration recorded in the near-source zone. There are undoubtedly many reasons for this. One may be attributed to the Icelandic building tradition leading to low-rise buildings of high specific strength. A second reason is undoubtedly related to earthquake preparedness carried out by companies, municipalities and individuals over the previous two decades. This experience indicates that earthquake risk can be reduced and managed through long-term planning, applying known earthquake engineering techniques, along with earthquake insurance to obtain economically acceptable results.

Acknowledgments. The National Power Company of Iceland, the Icelandic Public Road Administration, the City Engineer of Reykjavik and municipalities in South and North Iceland support the Icelandic Strong-motion Network. Special thanks go to our co-workers at the Engineering Research Centre in Selfoss, Iceland. Furthermore, the assistance of Dr J. Douglas and Professor N. N. Ambraseys is greatly appreciated. Thanks go to I. Cecic, M. Garcia-Fernandez and last but not least to Dr D. Slejko for inviting us to submit this paper to Bollettino di Geofisica Teorica ed Applicata. The corrections and suggestions by two referees improved the quality of the paper.

References

Ambraseys N.N. and Sigbjörnsson R.; 2000: *Re-appraisal of the seismicity of Iceland.* Polytechnica - Engineering seismology, Earthquake Engineering Research Centre, University of Iceland, 183 pp.

Ambraseys N.N., Smit P., Douglas J., Margaris B. Sigbjörnsson R., Ólafsson S., Suhadolc P. and Costa G.; 2003: *Internet site for european strong-motion data.* Boll. Geof. Teor. Appl., **44**, xx-xx.

Ambraseys N.N., Smit P., Sigbjornsson R., Suhadolc P. and Margaris B.; 2002: *ISESD – Internet site for european strong-motion data*. http://www.isesd.cv.ic.ac.uk, European Commission, Research-Directorate General, Environment and Climate Programme.

Anderson J.G. and Hough S.E.; 1984: *A model for the shape of the Fourier amplitude spectrum of acceleration at high frequencies.* Bull. Seismol. Soc. Am., **74**, 1969-1993.

Arias A.; 1970: *A measure of earthquake intensity.* In: Hansen R.J. (ed.), Seismic design of nuclear power plants, MIT Press, Cambridge, MA, pp. 438-483.

Boore D.M.; 1983: *Stochastic simulation of high-frequency ground motion based on seismological models of the radiated spectra.* Bull. Seismol. Soc. Am., **73**, 1865-1894.

Boore D.M., Joyner W.B. and Fumal T.E.; 1993: *Estimation of response spectra and peak accelerations from western North American earthquakes: An interim report.* Open-File Report 93-509. U.S. Geological Survey, 72 pp.

Brune J.; 1970: *Tectonic stress and the spectra of shear waves from earthquakes.* J. Geoph. Res., **75**, 4997-5009.

Brune J.; 1971: *Correction.* J. Geoph. Res., **76**, 5002.

Einarsson P.; 1991: *Earthquake and present-day tectonism in Iceland.* Tectonophysics, **189**, 261-279.

Einarsson Th.; 1994: *Geology of Iceland: rocks and landscape.* Mál og menning, Reykjavik, 335 pp.

Hanks T.C. and McGuire R.K.; 1981: *The character of high-frequency strong ground motion.* Bull. Seismol. Soc. Am., **71**, 2071-2095.

Ólafsson S.; 1999: *Estimation of earthquake-induced response.* Department of Structural Engineering, Norwegian University of Science and Technology, Trondheim, 140 pp.

Ólafsson S., Remseth S. and Sigbjörnsson R.; 2001: *Stochastic models for simulation of strong ground motion in Iceland.* Earthquake engineering and structural dynamics, **30**, 1305-1331.

Ólafsson S. and Sigbjörnsson R.; 1999: *A theoretical attenuation model for earthquake-induced ground motion.* Journal of earthquake engineering, **3**, 287-315.

Ólafsson S. and Sigbjörnsson R.; 2002: *Attenuation of strong-motion in the South Iceland earthquakes 2000.* In: Proceedings of the 12th European Conference on Earthquake Engineering, London, UK. Paper no. 123. Elsevier Science, 8 pp.

Ólafsson S., Sigbjörnsson R. and Einarsson P.; 1998: *Estimation of source parameters and Q from acceleration recorded in the Vatnafjöll Earthquake in South Iceland.* Bull. Seismol. Soc. Am., **88**, 556-563.

Sigbjörnsson R.; 1990: *Strong Motion Measurements in Iceland and Seismics Risk Assessment.* In: The Proceedings of the 9th European Conference on Earthquake Engineering, The Kucherenko Tsniisk of the USSR Gosstroy, Moscow, Vol. **10-A**, pp. 213-222.

Udias A.; 1999: *Principles of seismology.* Cambridge University Press, Cambridge, 475 pp.

Vanmarcke E.H. and Lai S.P.; 1980: *Strong motion duration and rms amplitude of earthquake records.* Bull. Seismol. Soc. Am., **70**, 1293-1307.

Thoroddsen Th.; 1899: *Landskjáftar á Sudurlandi.* Hid íslenzka bókmenntafélag, Copenhagen, 273 pp.

Thoroddsen Th.; 1925: *Die Geschichte der Isländischen Vulcane*. D. Kgl. Danske Vidensk. Selsk. Skrifter, Naturvidensk. og Matem. Afd., 8. Række, IX, 1-458.